# Nitrosation mechanisms, kinetics, and dynamics of the guanine and 9-methylguanine radical cations by nitric oxide — Radical-radical combination at different electron configurations

Jonathan Benny,[a,b] Toru Saito*[c], and Jianbo Liu*[a,b]

[a] Department of Chemistry and Biochemistry, Queens College of the City University of New York, 65-30 Kissena Blvd., Queens, NY 11367, USA;
[b] The Ph.D. Program in Chemistry, the Graduate Center of the City University of New York, 365 5th Ave., New York, NY 10016, USA;
[c] Department of Biomedical Information Science, Graduate School of Information Science, Hiroshima City University, 731-3194 Hiroshima, Japan

**Abstract** As a precursor to various reactive nitrogen species formed in biological systems, nitric oxide ($^{\bullet}$NO) participates in numerous processes, including enhancing DNA radiosensitivity in ionizing radiation-based radiotherapy. Forming guanine radical cations is another common DNA lesion resulting from ionization and oxidation damage. As such, the interaction of $^{\bullet}$NO with guanine radical cations ($G^{\bullet+}$) may contribute to the radiosensitization of $^{\bullet}$NO. An intriguing aspect of this process is the participation of multiple spin configurations in the reaction, including open-shell singlet $^{1,OS}[G^{\bullet+}(\uparrow)\cdots(\downarrow)^{\bullet}NO]$, closed-shell singlet $^{1,CS}[G(\uparrow\downarrow)\cdots NO^{+}]$, and triplet $^{3}[G^{\bullet+}(\uparrow)\cdots(\uparrow)^{\bullet}NO]$. In this study, the reactions of $^{\bullet}$NO with both unsubstituted guanine radical cations (in the $9HG^{\bullet+}$ conformation) and 9-methylguanine radical cations ($9MG^{\bullet+}$, a guanosine-mimicking model compound) were investigated in the absence and presence of monohydration of radical cations. Kinetic-energy dependent reaction product ions and cross sections were measured using an electrospray ionization guided-ion beam tandem mass spectrometer. The reaction mechanisms, kinetics, and dynamics were comprehended by interpreting the reaction potential energy surface using spin-projected density functional theory, coupled cluster theory, and multiconfiguration complete active space second-order perturbation theory, followed by RRKM kinetics modeling. The combined experimental and computational findings revealed closed-shell singlet $^{1,CS}[7\text{-NO-9MG}]^{+}$ as the major, exothermic product and triplet $^{3}[8\text{-NO-9MG}]^{+}$ as the minor, endothermic product. Singlet biradical products were not detected due to high reaction endothermicities, activation barriers, and inherent instability.

* Corresponding author email: jianbo.liu@qc.cuny.edu. Tel: 1-718-997-3271.
Co-corresponding author email: tsaito@hiroshima-cu.ac.jp.

## I. Introduction

Among the natural DNA nucleobases, guanine exhibits the lowest ionization[1, 2] and oxidation potential[3, 4] which renders it a dominant target in DNA for photolysis,[5, 6] ionizing[7, 8] and ion-beam radiation,[9] transition metal-mediated oxidation,[10] electrocatalytic oxidation,[11] and photooxidation.[12] The formation of guanine radical cations ($G^{\bullet+}$) as a result of these oxidative damages exacerbates DNA lesions.[13-18] A chemically and biologically relevant question arises regarding whether and how the $G^{\bullet+}$ lesion interacts with reactive oxygen species (ROS)[19] and reactive nitrogen species (RNS)[20, 21] generated during pathologic events. In recent years, our laboratory has investigated the oxidative modifications of $G^{\bullet+}$ by singlet $O_2$ (one of the major ROS in biological systems).[22-26] The present study expands our research to the reaction of $G^{\bullet+}$ with nitric oxide ($^{\bullet}NO$) radical.[21] The latter serves as a precursor to various RNS (e.g., $N_2O_3$, $ONOO^-$, transitional metal-nitrosyl) in biological systems.[21] The intriguing aspects of this radical-radical reaction are the formation, internal conversions (IC), and inter-system crossing (ISC) of multiple electron configurations (i.e., open-shell singlet, closed-shell singlet, and triplet), which controls reaction mechanisms and dynamics as demonstrated in our recent study on the spin-orbit charge transfer between $G^{\bullet+}$ and $^{\bullet}NO$ and the induced triplet-singlet ISC.[27] Charge transfer represents only one possible pathway in the radical-radical reaction. The complexity, variability, and versability of the reaction can manifest through other pathways that emerge as the radicals come into close proximity. In this work, we traced spin dynamics from singlet and triplet ion-molecule encounters through reaction precursors to covalent nitrosation adducts such as $[X\text{-}NO\text{-}G]^+$ (wherein a nitroso group -N=O is bonded to the X position at guanine), $[X\text{-}ON\text{-}G]^+$ (wherein the O terminal of -ON is bonded to the X position at guanine), $[X,Y\text{-}NO\text{-}G]^+$ and $[X,Y\text{-}ON\text{-}G]^+$ (wherein the N and O termini (or vice versa) of nitric oxide are cyclo-added to guanine across the X-Y bridge). We aimed to elucidate the roles that different spin configurations play in short-range interaction and combination of the two radicals. The biological relevance of this work is evident in the increased radiosensitivity of DNA in ionizing radiation-based radiotherapy in the presence of $^{\bullet}NO$.[28-38] Radiosensitization by $^{\bullet}NO$ arises from its reaction with short-

lived DNA radicals generated by radiation.[31, 34, 37, 39, 40] However, studies on this subject have been scarce, with existing literature primarily focusing on the reactions between •NO and the •OH adducts of purine and pyrimidine.[34, 40]

The present work started with the formation of the radical cations of guanine (in its O6-keto-N9H form, abbreviated as 9HG$^{\bullet+}$) and 9-methylguanine (abbreviated as 9MG$^{\bullet+}$, where the methyl group mimics the nucleoside sugar) in the gas phase, followed by the reactions of these radical cations with •NO under single-collision conditions provided in a guided-ion beam scattering experiment. The electronic structures and cross sections of product ions were determined as a function of kinetic energy. One of the primary objectives of this research was to benchmark theoretical methods capable of handling multireferential characters and non-adiabatic transitions in the reactions of doublet-doublet electronic states. To this end, experimental results were compared with reaction potential energies calculated using various theoretical approaches, including density functional theory (DFT), coupled cluster theory (CCSD),[41-43] multireference complete active space self-consistent field method (CASSCF),[44, 45] and complete active space second-order perturbation theory (CASMP2[46-48] and CASPT2[48, 49]). The combined experimental and computational findings were able to unveil explicit, electron configuration-dependent nitrosation mechanisms.

## II. Experimental and Computational Section

### A. Experimental Procedures

All chemicals used, including 2′-deoxyguanosine (dGuo, Sigma-Aldrich, > 99%), 9MG (Chemodex, > 98%), $Cu(NO_3)_2$ (Alfa Aesar, 99.999%), nitric oxide gas (Linde, > 99.5%), and HPLC-grade methanol and water, were purchased from commercial vendors and used without further purification. Ion-molecule reactions were carried out on a home-built guided-ion beam tandem mass spectrometer equipped with an electrospray ionization (ESI) source, a radiofrequency (rf) hexapole ion guide, a reactant quadrupole mass filter, an rf octopole ion guide surrounded by a scattering cell, a product quadrupole mass filter, and a pulse-counting electron multiplier detector. The apparatus and operational procedures were previously

published.[27, 50]

Following literature methods for producing radical cations of peptides and nucleosides,[51-53] $9HG^{\bullet+}$ was produced by collision-induced intramolecular electron-transfer dissociation of a $Cu^{II}$-nucleoside complex, i.e., $[Cu^{II}(dGuo)_3]^{\bullet2+} \rightarrow [Cu^{I}(dGuo)_2]^{+} + dGuo^{\bullet+}$ followed by cleavage of the N-glycosidic bond via $dGuo^{\bullet+} \rightarrow 9HG^{\bullet+} + C_5H_8O_3$. In the experiment, a mixture of 0.25 mM dGuo and 0.25 mM $Cu(NO_3)_2$ in methanol/water (v/v = 3:1) was electrosprayed into a heated (190 °C) desolvation capillary, which leads into the mass spectrometer source chamber. A 1.0-mm-diameter-orifice skimmer, positioned 3 mm from the capillary end, separates the source chamber and the hexapole ion guide. An electric field between the capillary (biased at 117 V with respect to ground) and the skimmer (biased at 18 V with respect to ground) prompted collision-induced dissociation of $[Cu^{II}(dGuo)_3]^{\bullet2+}$ formed in the electrospray to $dGuo^{\bullet+}$ and $9HG^{\bullet+}$, with the latter adopting the specific O6-keto-N9H conformer.[54, 55] Similarly, $9MG^{\bullet+}$ was produced by dissociation of $[Cu^{II}(9MG)_3]^{\bullet2+}$ formed from equimolar 0.25 mM 9MG and $Cu(NO_3)_2$ in methanol/water. The primary ion beam of $9HG^{\bullet+}$ had an intensity of $1 \times 10^5$ counts/sec, while that of $9MG^{\bullet+}$ had an intensity of $5 \times 10^5$ counts/sec. When the desolvation capillary was mildly heated (160 – 180 °C), monohydrated $9MG^{\bullet+}\cdot H_2O$ ($4 \times 10^4$ counts/sec) was produced alongside anhydrous radical cations.

The skimmed radical cation beam was directed into the hexapole ion guide for energy dampening and collisional focusing[56, 57] with the background gas at a pressure of ~ 20 mTorr. After passing the hexapole, ions were thermalized to a kinetic energy determined by the hexapole DC bias potential (1.0 V). Ions also exhibited 310 K Maxwell-Boltzmann vibrational ($E_{vib}$) and rotational ($E_{rot}$) energy distributions.[50] Radical ions of interest were then mass-selected by the reactant quadrupole mass filter and injected into the octopole ion guide that passes through an 11-cm-long scattering cell containing the nitric oxide target gas at a pressure of 0.02 mTorr. Similar to the hexapole, the octopole ion guide was operated with a combination of DC bias and rf potential. The rf potential trapped ions radially, while the DC potential accelerated or decelerated reactant ions at the octopole entrance to achieve the desired ion kinetic energy

in the laboratory frame ($E_{lab}$). The absolute zero and full width at half-maximum (FWHM) of $E_{lab}$ were calibrated by retarding potential measurements.[50, 58] The center-of-mass collision energy ($E_{CM}$) for the reaction of •NO with radical cations was determined by $E_{CM} = E_{lab} \times m_{neutral}/(m_{neutral} + m_{ion})$, where $m_{neutral}$ and $m_{ion}$ are the masses of the neutral and ionic reactants, respectively. The uncertainty for the absolute zero of $E_{lab}$ was < 0.1 eV, and the FWHM of $E_{lab}$ was 0.55 eV. These corresponded to an $E_{CM}$ uncertainty of ≤ 0.015 eV and FWHM of ≤ 0.09 eV. The nitrosation reaction was studied over an $E_{CM}$ range of 0.05 – 1.0 eV and under single ion-molecule collision conditions rendered by sufficiently low •NO gas pressure within the cell. Product ions and remaining reactant ions were collected by the octopole and refocused into the second quadrupole mass filter for analysis and counting. The thin-target collision condition allowed the calculation of reaction cross sections based on the ratio of product to reactant ion intensities, the •NO pressure in the scattering cell, and the effective cell length for collisions, following the Beer-Lambert law.[59, 60] Each experiment was repeated three times to determine the relative measurement uncertainty.

**B. Calculations**

**1. DFT geometry optimization**

Geometries of reactants, precursor complexes, transition states (TSs), and products for the reaction of $9MG^{\bullet+}$ with •NO were optimized using the DFT ωB97XD functional coupled with the 6-31+G(d,p) basis set. The range-separated ωB97XD functional mitigated self-interaction errors and improved the orbital description of radical cations.[61] To distinguish between open- and closed-shell singlet structures, singlet biradicals were computed using the broken symmetry (BS) unrestricted DFT with the guess = mix option (i.e., mixing HOMO and LUMO to break α-β and spatial symmetries in an initial guess),[62] whereas closed-shell singlet structures were computed using restricted DFT. All TSs exhibited only one imaginary frequency, consistent with expected reaction pathways. Intrinsic reaction coordinate (IRC) calculation was carried out for each TS to verify that it connects to the correct reactant and product structures.

DFT calculations were conducted using Gaussian 16.[63] Reaction enthalpies (ΔH) were computed at

298 K, incorporating zero-point energies (ZPEs, scaled by 0.975[64]) and thermal corrections. Atomic charges, spin densities, and α- and ß-spins were analyzed using the Natural Orbital Analysis Program NBO 6.0.[65] A computational difficulty arose due to the open-shell, multi-reference character of •NO, which is akin to triplet instability in a doublet system.[66, 67] Consequently, the ωB97XD/6-31+G(d,p) method overestimated the ionization energy (IE) of •NO by 0.5 eV compared to the experimental adiabatic IE (9.2643 eV ± 0.0005 eV, measured by pulsed-field ionization photoelectron spectroscopy),[68] as shown in Table S1 in the Supporting Information. For this reason, the DFT energy of the •NO reactant was obtained by subtracting the experimental IE(•NO) from the DFT energy of $NO^+$.

**2. Assessment of spin contamination using coupled-cluster theory**

T1 diagnostic[69, 70] for spin contamination in DFT-optimized reaction structures was carried out using the domain-based local pair-natural orbital coupled-cluster method with single, double, and perturbative triple excitations (DLPNO-CCSD(T))[71, 72] paired with the aug-cc-pVTZ basis set. The T1 value was calculated by $T1 = \|t_1\|/\sqrt{n}$, where $\|t_1\|$ is the Frobenius norm of the single-excitation amplitude vector and $n$ is the number of correlating electrons.[69] $T1$ of < 0.02 for closed-shell systems and < 0.03 for open-shell systems indicates minimal spin contamination, $T1$ ranging from 0.06 to 0.07 indicates moderate multireference character, and $T1$ of ≥ 0.16 indicates severe multireference character.[73] DLPNO-CCSD(T) has been validated against the gold standard method CCSD(T).[41-43] The comparisons have demonstrated an accuracy of 4 kJ/mol or better for DLPNO-CCSD(T) in estimating reaction enthalpies[74, 75] and barriers.[73, 76] The inclusion of perturbative correction for triple excitation helps mitigate deficiencies arising from a single-determinant reference, enabling DLPNO-CCSD(T) to effectively manage moderate spin contamination.

DLPNO-CCSD(T) calculations were carried out using ORCA 4.2,[77, 78] with the NormalPNO (pair natural orbital) parameters[73, 74] of TCutPair = $10^{-4}$, TCutPNO = $3.3 \times 10^{-7}$, and TCutMKN = $10^{-3}$. The DLPNO-CCSD(T)-calculated IE(•NO) (9.20 eV, see Table S1 in the Supporting Information) is only 0.06 eV less than the experimental value.

### 3. Spin purification using approximate spin projection

Open-shell singlets are prone to spin contamination in unrestricted DFT calculations,[79] therefore Yamaguchi′s approximate spin projection (AP)[27, 80-82] was utilized for spin purification in energy calculations as $E = \frac{\langle \hat{\mathbf{S}}^2 \rangle^{\mathrm{HS}}}{\langle \hat{\mathbf{S}}^2 \rangle^{\mathrm{HS}} - \langle \hat{\mathbf{S}}^2 \rangle^{\mathrm{BS}}} E^{\mathrm{BS}} - \frac{\langle \hat{\mathbf{S}}^2 \rangle^{\mathrm{BS}}}{\langle \hat{\mathbf{S}}^2 \rangle^{\mathrm{HS}} - \langle \hat{\mathbf{S}}^2 \rangle^{\mathrm{BS}}} E^{\mathrm{HS}}$, where $E^{\mathrm{BS}}$ and $\langle \hat{\mathbf{S}}^2 \rangle^{\mathrm{BS}}$ represent the total energy and the expectation value of the total spin angular momentum operator for a target broken-symmetry singlet, and $E^{\mathrm{HS}}$ and $\langle \hat{\mathbf{S}}^2 \rangle^{\mathrm{HS}}$ are the counterparts for the triplet.

### 4. Complete active space second-order perturbation theory

Reaction energies were further explored using CASSCF[44, 45] coupled with the 6-31+G(d,p) basis set. Active spaces were defined as (9,7) for 9MG$^{\bullet+}$, (11,8) for $^{\bullet}$NO, and (20,15) for adducts, including critical orbitals $\sigma_{O(2s)\text{-}N(2s)}$, $\sigma^*_{O(2s)\text{-}N(2s)}$, $2 \times \pi_{O(2p)\text{-}N(2p)}$, $\sigma_{O(2p)\text{-}N(2p)}$, $2 \times \pi^*_{O(2p)\text{-}N(2p)}$, and $\sigma^*_{O(2p)\text{-}N(2p)}$ in $^{\bullet}$NO, as well as the $\pi$ and $\sigma_{N-H}$ in 9MG$^{\bullet+}$. However, CASSCF significantly underestimated IE($^{\bullet}$NO) (see Table S1 in the Supporting Information), likely because it included primarily nondynamic electronic correlation. To capture a significant part of dynamic correlation energy, second-order Møller-Plesset perturbation theory was incorporated by using CASMP2.[46-48] Pople basis sets 6-31+G(d,p), 6-311+G(d,p), and 6-311++G(d,p), and the atomic natural orbital-relativistic core-correlated valence triple-ξ plus polarization functions ANO-RCC-VTZP[83, 84] were employed for the CASMP2 calculations of IE. Surprisingly, computational errors escalated notably with the expansion of the basis set, as listed in Table S1 in the Supporting Information. The CASMP2 seems to have achieved the best result for IE($^{\bullet}$NO) (9.06 eV) with the 6-31+G(d,p) basis set, albeit potentially fortuitous.

To rectify these issues, an alternative version of the complete active space perturbation theory, CASPT2,[48, 49] was adopted. A potential drawback of CASPT2 concerns an intruder state in which the zeroth-order energy associated with the CASSCF wavefunction is nearly equal to that of a perturber (correction function).[85] This problem was reduced by adopting an imaginary shift correction (0.1).[86] In addition, an ionization potential-electron affinity (IPEA) shift parameter (0.25 a.u.)[87] was applied to

balance descriptions of open- and closed-shell configurations in the zeroth-order Hamiltonian.[88] The IE(•NO) of 9.12eV (see Table S1 in the Supporting Information), calculated using a combination of CASPT2 and the ANO-L-VTZP basis set (it contains the same primitive basis functions as ANO-RCC but differs in contraction coefficient, which is determined for nonrelativistic calculations),[89, 90] showed good agreement with the experimental value.

CASSCF and CASMP2 calculations were carried out using Gaussian 16,[63] with the ANO-RCC-VTZP orbital obtained from the Basis Set Exchange.[91] CASPT2 calculations were carried out using OpenMolcas 23.10.[92, 93] Reaction enthalpies reported at CASPT2/ANO-L-VTZP included the CASPT2-calculated electronic energy and the 298 K thermal correction calculated at ωB97XD/6-31+G(d,p) (including scaled ZPE).

**5. Unimolecular kinetics modeling**

Rice-Ramsperger-Kassel-Marcus (RRKM) theory[94] densities of states (DOS) and rate constants were calculated using the direct count algorithm[95] available in the RRKM code of Zhu and Hase[96] and the scaled frequencies, energies, and moments of inertia of the complexes and TSs determined from the CASPT2/ANO-L-VTZP//ωB97XD/6-31+G(d,p) calculations. For reactions involving no reverse barrier, orbit transition states[97] were assumed. The orbital angular momentum $L$ for the reaction was determined from collision cross section ($\sigma_{\text{collision}}$), i.e., $L = \mu \cdot v_{rel} \cdot \sqrt{\sigma_{collision}/\pi}$ where $\mu$ and $v_{\text{rel}}$ are the reduced mass and relative velocity for collision partners, respectively.

**III. Experimental Results**

As previously reported,[22, 98] the lowest-energy structures of 9HG$^{\bullet+}$ and 9MG$^{\bullet+}$ adopt a O6-keto-conformation, and each had an overwhelmingly dominant population in the ion beam. Note that the O6-keto-N7H isomer of the guanine radical cation (abbreviated as 7HG$^{\bullet+}$) lies at an energy of 0.11 eV higher than 9HG$^{\bullet+}$. We also note that the radical cations were generated during ion transfer within the source chamber under relatively high background gas pressure (1.6 Torr, predominantly air with a small fraction of solvent vapor). There was a possibility that radical cations underwent solvent-assisted isomerization.[99]

Despite this, the majority of 9HG$^{\bullet+}$ and 9MG$^{\bullet+}$ were expected to retain an O6-keto-N9H or O6-keto-N9-$CH_3$ structure due to thermalization within the hexapole, where any higher-energy isomers would relax to equilibrium populations at 310 K. Additionally, our CID experiments of various base pairs containing 9MG$^{\bullet+}$ confirmed that only conformers containing an O6-keto-N9-$CH_3$ structure match the measured dissociation threshold energies.[100,101]

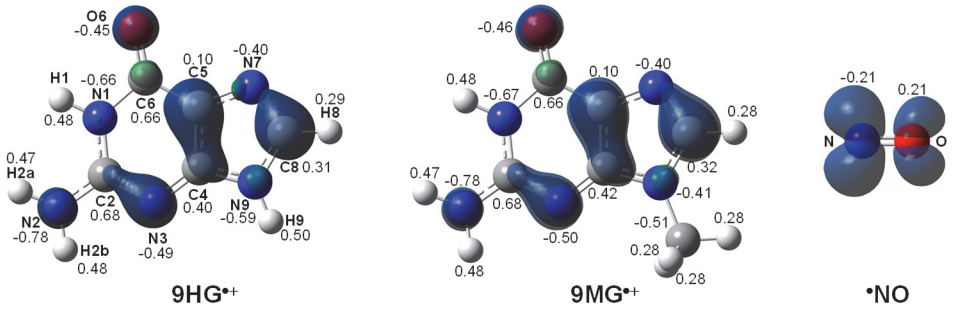


**Scheme 1.** Structures of 9HG$^{\bullet+}$, 9MG$^{\bullet+}$, and $^{\bullet}$NO with atomic numbering schemes. Spin (contour plots) and atomic charge (numbers) were calculated using NBO 6.0 at the ωB97XD/6-31+G(d,p) level of theory.

Scheme 1 illustrates the structures of reactants along with their NBO charge and spin density distributions. Both 9HG$^{\bullet+}$ and 9MG$^{\bullet+}$ delocalize the unpaired electron spin mainly among the N3, C5, and C8 positions and the positive charge among C2, C4, and C8. Consequently, it seems reasonable to infer that the N9-methyl substitution would not have a significant effect on the structures for guanine nitrosation.

### A. Reaction of $^{\bullet}$NO with 9HG$^{\bullet+}$

We reported previously that the collisions of 9HG$^{\bullet+}$ (and 9MG$^{\bullet+}$) with $^{\bullet}$NO produced a charge-transfer product pair of 9HG (9MG) + $NO^+$ at $E_{CM} \geq 1.5$ eV.[27] The present experiment thus specifically focused on measuring the formation of nitrosation complexes at low energies. Figure 1 depicts the reaction product ion cross section for 9HG$^{\bullet+}$ (*m/z* 151) + $^{\bullet}$NO as a function of kinetic energy. Error bars were derived from three sets of measurements. Product ions were detected at *m/z* 181, which corresponds to a covalent [NO-9HG]$^+$ adduct. The product cross section reaches a maximum at the lowest experimental kinetic energy and decreases monotonically with increasing kinetic energy. No complex

ions were detected above $E_{CM}$ of 0.5 eV. This kinetic energy dependence indicates an exothermic reaction without an activation barrier above the reactants.

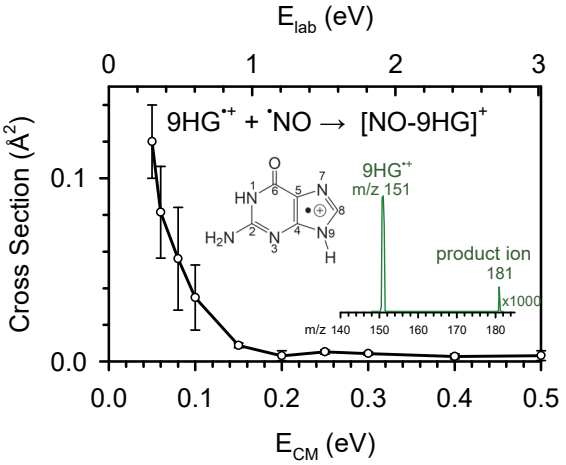


**Fig. 1.** Product ion cross section for the reaction of 9HG$^{\bullet+}$ + $^{\bullet}$NO as a function of kinetic energy in the center-of-mass frame ($E_{CM}$, bottom axis) and laboratory frame ($E_{lab}$, top axis). Insets show the Chemdraw for 9HG$^{\bullet+}$, and product ion mass spectrum recorded at $E_{CM}$ = 0.05 eV.

### B. Reaction of $^{\bullet}$NO with 9MG$^{\bullet+}$

9MG$^{\bullet+}$ was chosen as a model compound for dGuo$^{\bullet+}$ with the bulky ribose sugar substituted by a methyl group. Figure 2a presents the nitrosation product cross section for 9MG$^{\bullet+}$ (*m*/z 165), measured as a function of $E_{CM}$ from 0.05 to 1.0 eV. The reaction efficiency, estimated by $\sigma_{reaction}/\sigma_{collision}$ (where $\sigma_{collision}$ represents the ion-induced dipole capture cross section[102] or hard-sphere collision cross section calculated using the orientation-averaged projected area method of the IMoS program,[103, 104] whichever is larger), is ~0.01% at $E_{CM}$ = 0.05 eV, quickly decreasing to 0.003% at $E_{CM}$ = 0.1 eV. For comparison, the reaction efficiency for 9HG$^{\bullet+}$ is 0.1% at $E_{CM}$ = 0.05 eV, decreasing to 0.05% at 0.1 eV.

An intriguing finding in the nitrosation of 9MG$^{\bullet+}$ is the emergence of a distinct, endothermic product channel. The cross section for this product channel starts to rise at $E_{CM}$ = 0.2 eV, reaches its maximum at 0.22 eV, and then gradually decreases, becoming negligible at energies above 0.8 eV. Notably, this specific product channel is not prominently observed in the reaction of 9HG$^{\bullet+}$ + $^{\bullet}$NO in Figure 1 — there is a possibility that this channel has been overshadowed by the relatively large exothermic product channel for 9HG$^{\bullet+}$.

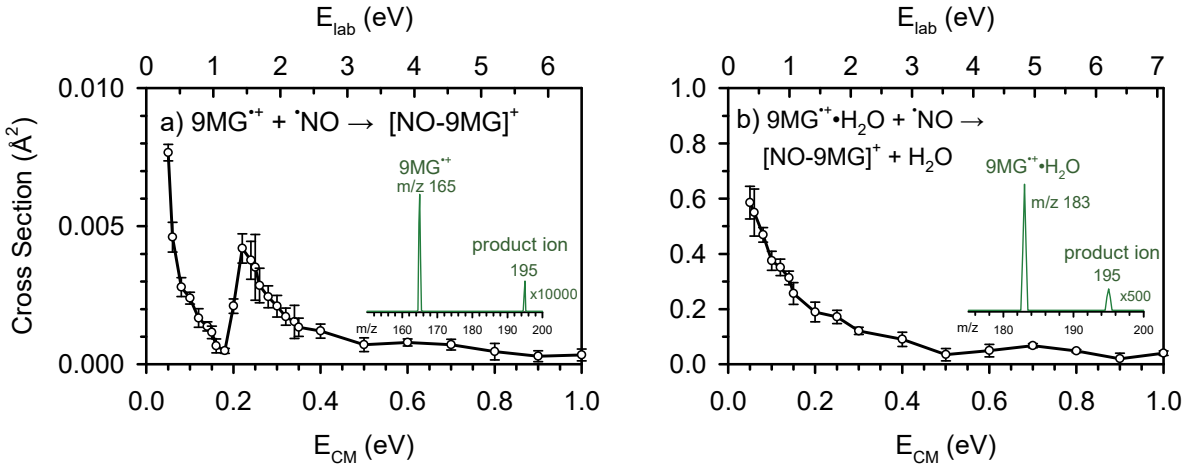


**Fig. 2.** Product ion cross section for the reactions of •NO with (a) 9MG•+ and (b) 9MG•+·H$_2$O as a function of kinetic energy in the center-of-mass frame ($E_{CM}$, bottom axis) and laboratory frame ($E_{lab}$, top axis). Insets show product ion mass spectra recorded at $E_{CM}$ = 0.05 eV.

Despite the similar kinetic energy dependence, the reaction efficiency of 9MG•+ with •NO appears to be an order of magnitude lower than that of 9HG•+. It is plausible that, due to insufficient energy relaxation in the rarefied gas-phase environment, a fraction of the adducts formed through an exothermic reaction might have decomposed into the starting reactants before reaching the mass spectrometer detector (the ion time-of-flight time was 100 – 500 μs within the mass spectrometer). Similar decomposition scenario was observed in the $^1O_2$ addition reactions of 9MG•+ and 8-bromo-9HG•+.[22, 24]

No proton-transfer (PT) or hydrogen-transfer (HT) was observed between 9HG•+/9MG•+ and •NO within the experimental energy range. According to ωB97XD/6-31+G(d,p) calculations, the PT ΔH (298 K) leading to $^2$[9MG – H$_{N1}$]• + HNO+ is 4.27 eV and that to $^2$[9MG – H$_{N1}$]• + HON+ is 4.88 eV. The HT ΔH (298 K) leading to [9MG – H$_{N2}$]+ + HNO is 2.08 eV and that to [9MG – H$_{N2}$]+ + $^3$HON is 2.92 eV.

### C. Reaction of •NO with 9MG•+·H$_2$O

Since the extremely low reaction efficiency observed for 9MG•+ with •NO might be possibly attributed to the decomposition of nascent nitrosation adducts carrying the reaction′s exothermicity, we adopted a workaround by using the monohydrated 9MG•+·H$_2$O as reactant ions for collisions with •NO. In this modified reaction system, the heat release from nitrosation, which could otherwise lead to the

decomposition of $[NO\text{-}9MG]^+$ in dry conditions, instead facilitated the elimination of the water ligand along with the release of product kinetic energy.[22, 24, 105] The anticipated outcome was verified in the experiment.

As shown in Figure 2b, product ions for $9MG^{\bullet+}\cdot H_2O$ (*m/z* 183) + $^{\bullet}NO$ were detected at *m/z* = 195, which corresponds to the liberation of a water ligand from the $^{\bullet}NO$-adduct of $9MG^{\bullet+}\cdot H_2O$. The reaction efficiency for $9MG^{\bullet+}\cdot H_2O$ is 0.54% at $E_{CM}$ = 0.05 eV, decreasing to 0.5% at 0.1 eV. Thus, the complex formation of $9MG^{\bullet+}\cdot H_2O$ + $^{\bullet}NO$ increases by two orders of magnitude than that of dry $9MG^{\bullet+}$ + $^{\bullet}NO$.

The detection of the exothermic reaction of $9MG^{\bullet+}\cdot H_2O$ + $^{\bullet}NO \rightarrow [NO\text{-}9MG]^+ + H_2O$ has imposed a constraint on the exothermicity of the reaction — it must exceed the water-binding energy of $9MG^{\bullet+}\cdot H_2O$. The water-binding energy depends on the hydration structure (see Figure S1 in the Supporting Information). It is 0.48 eV when water is H-bonded to a N2-H in 9MG (i.e., referred to as W2), 0.58 eV when water is double H-bonded to N1-H and O6 (i.e., W16), and 0.68 eV when water is double H-bonded to N1-H and N2-H (i.e., W12).[98, 106] According to direct dynamics trajectory simulations for $9MG^{\bullet+}$ hydration,[98, 106] the W12 binding motif represents the most probable structure for $9MG^{\bullet+}\cdot H_2O$. The implication is that the cross section in Figure 2b should be mostly attributed to the reaction of the W12 structure of $9MG^{\bullet+}\cdot H_2O$. It follows that the nitrosation enthalpy of $9MG^{\bullet+}$ should exceed 0.68 eV.

Since the exothermic nitrosation product for $9MG^{\bullet+}\cdot H_2O$ + $^{\bullet}NO$ remains dominant up to $E_{CM}$ = 0.5 eV, the endothermic product, which would be otherwise observable between 0.2 and 0.5 eV, becomes obscured as reactant hydration could not enhance an endothermic reaction.

## IV. Theoretical Results

### A. Spin dynamics

As $9MG^{\bullet+}$ more closely resembles $dGuo^{\bullet+}$ in terms of structure and distributions of spin and charge than $9HG^{\bullet+}$,[22, 98] $9MG^{\bullet+}$ was chosen as a prototypical system for computational modeling. Figure 3 presents a relaxed potential energy surface (PES) for $9MG^{\bullet+}$ + $^{\bullet}NO$. Since the N-terminal of $^{\bullet}NO$ holds

the radical electron and thus has greater reactivity toward $9MG^{\bullet+}$ than the O-terminal, PES was calculated along the distance (r[9MG-N]) between the center-of-mass of 9MG and the N-terminal of $^{\bullet}NO$. The PES scans from r[9MG–N] = 15 Å to 1.8 Å (at a step size of 0.01 Å from 1.8 to 5 – 6.5 Å and 0.1 Å afterwards) using the ωB97XD/6-31+G(d,p) method. The PES includes three electron configurations: an open-shell singlet $^{1,OS}[9MG^{\bullet+}(\uparrow)\cdots(\downarrow)^{\bullet}NO]$ (black color PES in Figure 3), a closed-shell singlet $^{1,CS}[9MG(\uparrow\downarrow)\cdots NO^{+}]$ (red), and a triplet $^{3}[9MG^{\bullet+}(\uparrow)\cdots(\uparrow)^{\bullet}NO]$ (blue). The surface for $^{1,OS}[9MG^{\bullet+}(\uparrow)\cdots(\downarrow)^{\bullet}NO]$ was corrected for spin contamination using approximate spin projection. Spin dynamics for the radical-radical combination varies at different stages of the reaction as described below:

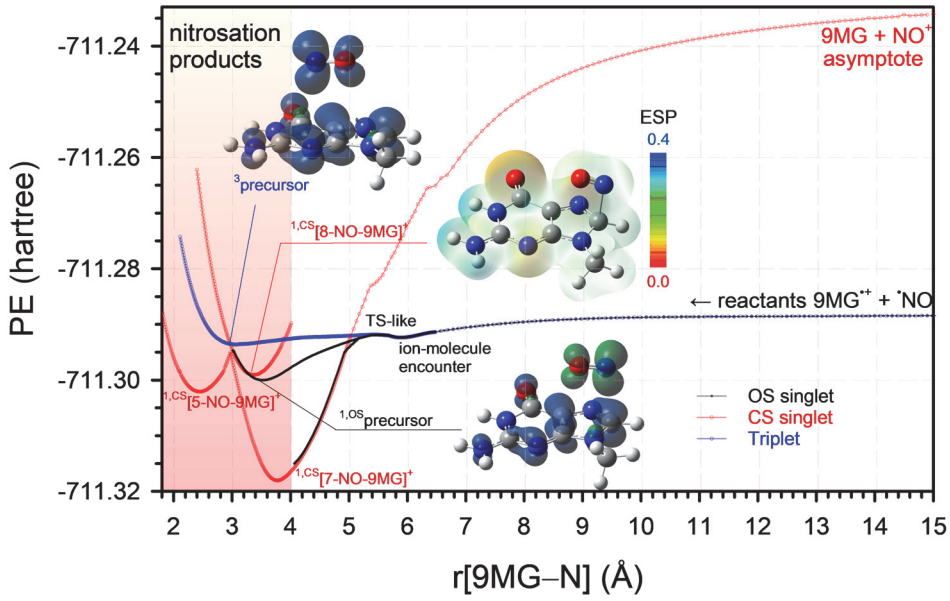


**Fig. 3.** PES for $9MG^{\bullet+}$ + $^{\bullet}NO$ vs. r[9MG–N] (the distance between the center-of-mass of $9MG^{\bullet+}$ and the N of $^{\bullet}NO$), calculated at the ωB97XD/6-31+G(d,p) level of theory. Electronic states are distinguished by colors: black for open-shell (OS) singlet, red for closed-shell (CS) singlet, and blue for triplet. Insets illustrate $^{1,OS}$precursor and $^{3}$precursor (C: gray; H: white; N: blue; and O: red) with spin density contour plot, and $^{1,CS}[8\text{-NO-9MG}]^{+}$ with electrostatic potential (ESP, in eV)-fitted charge distribution.

1) At the beginning of collisions, the radicals assemble into either $^{1,OS}[9MG^{\bullet+}(\uparrow)\cdots(\downarrow)^{\bullet}NO]$ or $^{3}[9MG^{\bullet+}(\uparrow)\cdots(\uparrow)^{\bullet}NO]$. The two electronic states are energetically degenerate at long separation until r[9MG–N] reaches 5 Å from which the open-shell singlet becomes lower in energy than the triplet. Interaction in the ion-molecule encounter (mostly ion-dipole interaction) starts to become significant at the shallow PES minimum located at [9MG–N] = 5.8 Å. The structure of this encounter is shown in the

Supporting Information, where the $^{\bullet}$NO is approaching the 9MG$^{\bullet+}$ in a parallel direction. The electrostatic binding energy of this encounter is 0.11 eV. The encounter rearranges structure at a TS-like point with a forward barrier of 0.03 eV. The TS-like structure is also shown in the Supporting Information, where the $^{\bullet}$NO moiety moves over 9MG$^{\bullet+}$ to prepare for the formation of a stable [NO-9MG]$^{+}$ complex.

2) Singlet reactions. The TS-like point marks the starting point where the paths of $^{1,OS}$[9MG$^{\bullet+}$(↑)···(↓)$^{\bullet}$NO] and $^{3}$[9MG$^{\bullet+}$(↑)··· (↑)$^{\bullet}$NO] diverge. Depending on reaction orientation: $^{1,OS}$[9MG$^{\bullet+}$(↑)···(↓)$^{\bullet}$NO] may form an electrostatically bonded complex at r[9MG-N] = 3.5 Å, referred to as $^{1,OS}$precursor (shown in the bottom inset of Figure 3). The $^{1,OS}$precursor may converge to a singlet closed-shell $^{1,CS}$[8-NO-9MG]$^{+}$, wherein the positive charge is distributed over the entire complex, as manifested by the electrostatic potential (ESP)-fitted charge distribution in the middle inset of Figure 3. Alternatively, the $^{1,OS}$[9MG$^{\bullet+}$(↑)···(↓)$^{\bullet}$NO] may converge to a singlet closed-shell $^{1,CS}$[7-NO-9MG]$^{+}$ at [9MG–N] = 3.7 Å, and the latter may interconvert to $^{1,CS}$[5-NO-9MG]$^{+}$. The $^{1,CS}$[5-NO-9MG]$^{+}$, $^{1,CS}$[7-NO-9MG]$^{+}$, and $^{1,CS}$[8-NO-9MG]$^{+}$ act as hubs for interconversion to other singlet nitrosation products to be described below.

3) Triplet reactions. The nitrosation reaction may also initiate from $^{3}$[9MG$^{\bullet+}$(↑)···(↑)$^{\bullet}$NO]. The triplet first forms an electrostatically bonded complex at r[9MG–N] = 3 Å, referred to as $^{3}$precursor. The spin sites of $^{3}$precursor are characterized in the upper left inset of Figure 3. The charge of $^{3}$precursor, however, remains at 9MG. Similar to $^{1,OS}$precursor, $^{3}$precursor allows for repeated encounters between reactants; consequently, the system proceeds to form various triplet nitrosation structures to be described below. As reported in our previous study,[27] $^{3}$[9MG$^{\bullet+}$(↑)··· (↑)$^{\bullet}$NO] may undergo spin-orbit charge transfer at [9MG–N] = 5 Å and become correlated to the charge transfer (CT) asymptote 9MG + NO$^{+}$.

**B. Nitrosation pathways and energetics**

Guided by spin dynamics, we mapped out possible nitrosation pathways using ωB97XD/6-31+G(d,p). Results are illustrated using flow charts in Schemes 2 – 4. Cartesian coordinates for reaction structures are provided in the Supporting Information. Scheme 2 presents three distinctive types of NO-additions

leading from $^{1,OS}$precursor to a closed-shell singlet product. The N-terminal addition of •NO (illustrated in black) at the N7 and C8 positions produces $^{1,CS}$[7-NO-9MG]$^+$ and $^{1,CS}$[8-NO-9MG]$^+$, respectively. $^{1,CS}$[7-NO-9MG]$^+$ may convert to $^{1,CS}$[5-NO-9MG]$^+$ and subsequently to $^{1,CS}$[3-NO-9MG]$^+$, and $^{1,CS}$[8-NO-9MG]$^+$ may convert to $^{1,CS}$[7H-8-NO-9MG]$^+$ via intra-molecular proton transfer. The N-terminal addition also produces $^{1}$[2-NHNO-3H-9MG]$^+$ accompanied by a proton transfer from N2 to N3. The O-terminal addition of •NO (illustrated in blue) occurs only at C8, leading to the formation of $^{1}$[7H-8-ON-9MG]$^+$ with a simultaneous hydrogen transfer from C8-H to N7. Cycloadditions (illustrated in red) were identified for $^{1,CS}$[4,5-NO-9MG]$^+$ and $^{1,CS}$[7,8-NO-9MG]$^+$. While both cycloadditions were mediated by a single TS, the reactions may be characterized as asynchronous concerted: although the cycloaddition involves no intermediate (i.e., concerted), it comprises two "events" that do not occur simultaneously (i.e., asynchronous). For example, the addition of the N-terminal to C4 precedes the addition of the O-terminal to C5 in the formation of $^{1,CS}$[4,5-NO-9MG]$^+$.

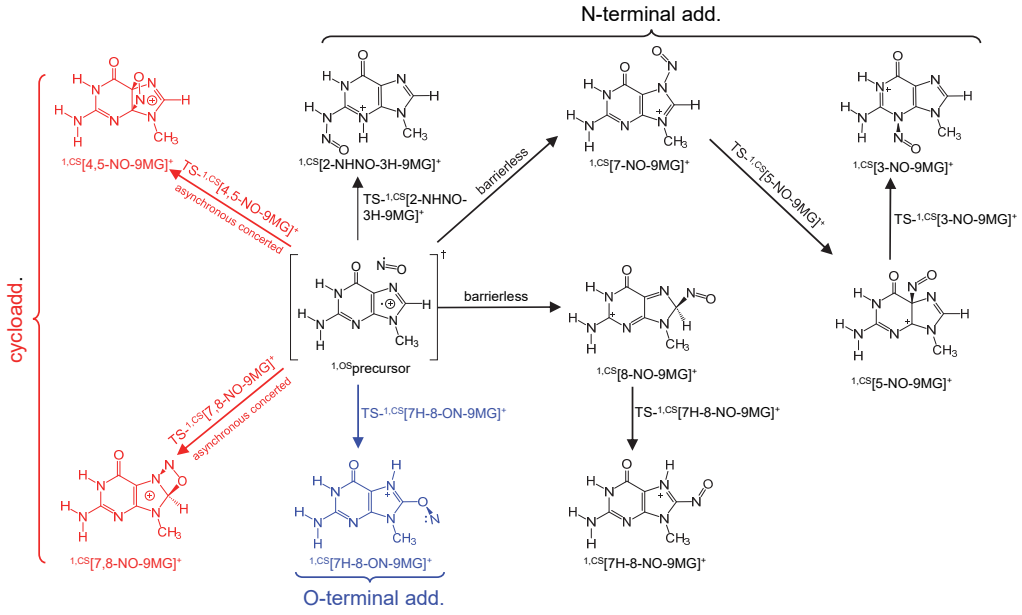


**Scheme 2.** Probable nitrosation pathways and products of 9MG$^{•+}$ in the closed-shell singlet state.

Compared to the closed-shell singlet, the open-shell singlet presents fewer pathways, as depicted in Scheme 3. An O-terminal addition pathway leads to a $^{1,OS}$[8-ȮṄ-9MG]$^+$ biradical, and the latter may interconvert to a $^{1,OS}$[7H-8-ȮṄ-9MG]$^+$ biradical via a hydrogen transfer. Additionally, four cycloadditions

were identified. Only $^{1,OS}$[7,8-ON-9MG]$^+$ forms via an asynchronous concerted route starting with the 8-NO addition in $^{1,OS}$precursor, whereas $^{1,OS}$[2,4-NO-9MG]$^+$, $^{1,OS}$[5,8- NO-9MG]$^+$, and $^{1,OS}$[5,8-ON-9MG]$^+$ are all synchronous cycloadditions.

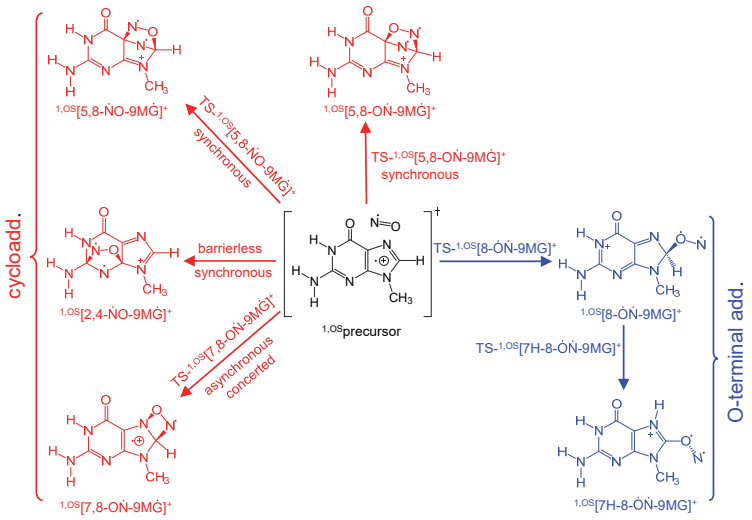


**Scheme 3.** Probable nitrosation pathways and products of 9MG$^{\bullet+}$ in the open-shell singlet state, wherein unpaired electrons are indicated in the Chemdraw structures and formulas.

Of the three electronic states, the triplet presents the most versatile pathways. The top frame of Scheme 4 presents various N- vs. O-terminal additions of $^{\bullet}$NO to 9MG$^{\bullet+}$. The bottom frame presents concerted and sequential cycloadditions: the formation of $^3$[4,5-ON-9MG]$^+$, $^3$[5,8-ON-9MG]$^+$, and $^3$[7,8-ON-9MG]$^+$ is asynchronous, the formation of $^3$[2,4-NO-9MG]$^+$ and $^3$[7,8-NO-9MG]$^+$ is synchronous, and the formation of $^3$[5,8-NO-9MG]$^+$ can be either.

It is interesting to compare spin locations in the open-shell singlet vs. triplet products. In the singlet O-terminal adducts, two unpaired electrons are each located at N and O of NO; whereas in the singlet biradical cycloadducts, two unpaired electrons each remain at 9MG$^{\bullet+}$ and $^{\bullet}$NO, respectively. In the triplet N-terminal adducts, the unpaired electron of 9MG$^{\bullet+}$ shifts to the O of NO. In the triplet O-terminal adducts, the unpaired electron of 9MG$^{\bullet+}$ shifts to the N of NO, resulting in both unpaired electrons being located at the N-terminal. Finally, in the triplet cycloadducts, two unpaired electrons are each retained at 9MG$^{\bullet+}$ and $^{\bullet}$NO. Regardless of product electronic states, the charge largely remains at 9MG.

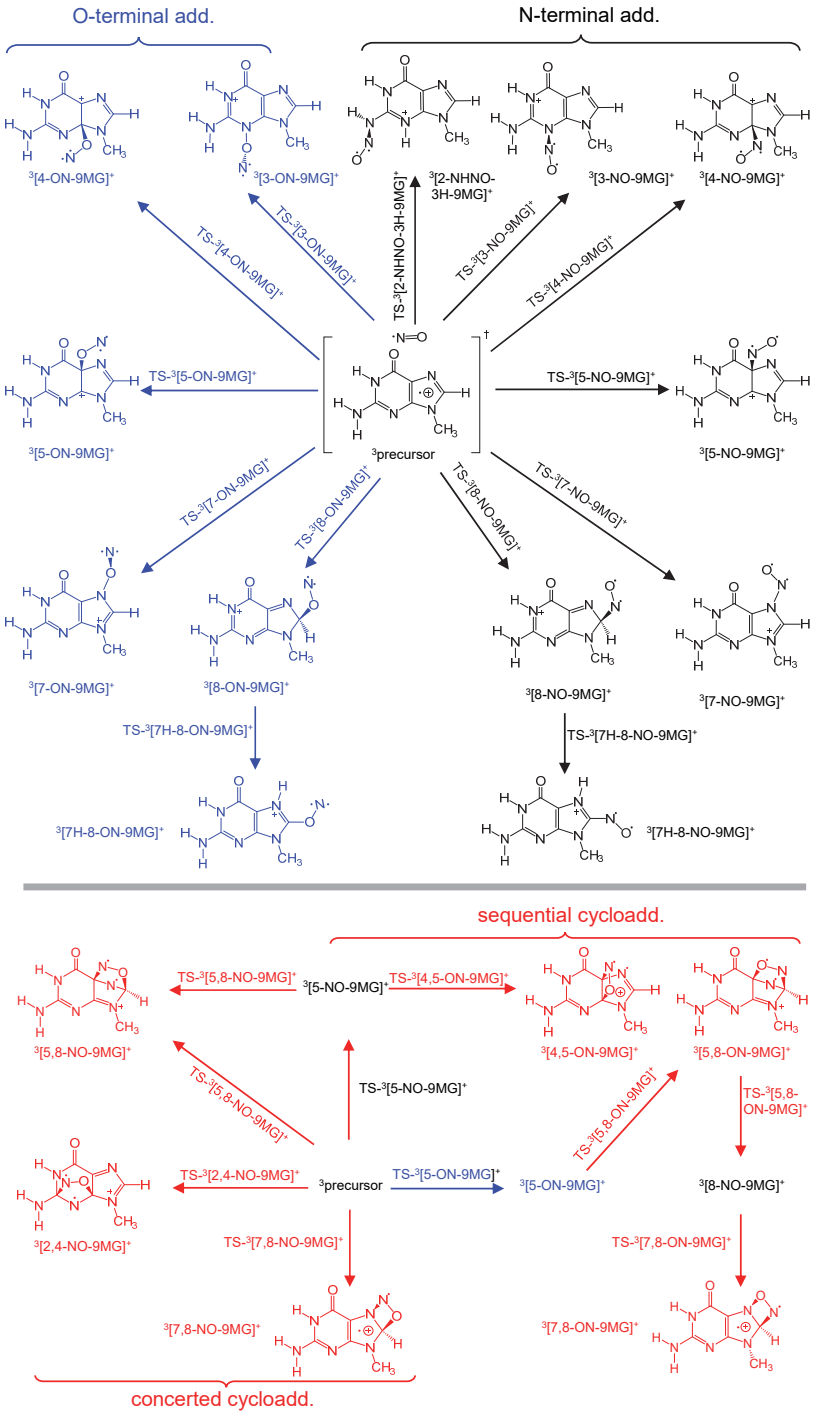


**Scheme 4.** Probable nitrosation pathways and products of 9MG$^{\bullet+}$ in the triplet state.

Tables S2 and S3 in the Supporting Information compare 298 K reaction enthalpies calculated at the DFT, DLPNO-CCSD(T)/aug-cc-pVTZ, and CASPT2/ANO-L-VTZP levels, and $< \widehat{S^2} >$ and T1 diagnostic for reaction structures. All calculations used the ωB97XD/6-31+G(d,p)-optimized reaction structures.

All closed-shell singlet structures have a $<\widehat{S^2}>$ value of 0.00 and $T1 \leq 0.019$ and all triplet structures have a $<\widehat{S^2}>$ of 2.00 and $T1 \leq 0.023$, which indicates at most minor spin contamination for these species. On the other hand, biradical structures have a $<\widehat{S^2}>$ of 0.83 – 1.01, which represents a diradical character in a range of 59 – 100% (using diradical index[62] $n_{DC} = \left(1 - \sqrt{(1-<\widehat{S^2}>}\right) \times 100\%$).

Compared to the CASPT2 results, the ωB97XD level has underestimated the reaction energies by 0.2 – 0.4 eV whereas the DLPNO-CCSD(T) level has overestimated the energies by 0.4 – 0.6 eV. The transition state TS-$^{1,CS}$[4,5-NO-9MG]$^+$ for 4,5-cycloaddition shifts to an energy below the product at the CASPT2 level, indicating that this cycloaddition is barrierless. All theories have predicted that exothermic nitrosation pathways occur only in the closed-shell singlet, as the latter represents the ground electronic state; and all open-shell singlet and triplet pathways are either endothermic or have activation barriers above reactants, indicating that these electronic states are not thermodynamically favorable as expected from the Pauli exclusion principle.

## V. Discussion

### A. $^{1,CS}$[7-NO-9MG]$^+$ represents the only exothermic nitration product

Figure 4 compiles potential energies for the formation and interconversions of all nitrosation reactions mediated by the open- and closed-shell singlets. As aforementioned, the H-binding energy of 9MG$^{\bullet+}$·$H_2O$ ranges from 0.48 to 0.68 eV, of which 0.68 eV is the most probable. This has imposed a constraint on the minimum and the most probable exothermicity range for experimentally measured products, as marked in the Y-axis of Figure 4. Accordingly, the most probable product ions correspond to $^{1,CS}$[7-NO-9MG]$^+$. This agrees with the relaxed PES in Figure 3, where $^{1,CS}$[7-NO-9MG]$^+$ represents the first covalent structure as reactants approach each other.

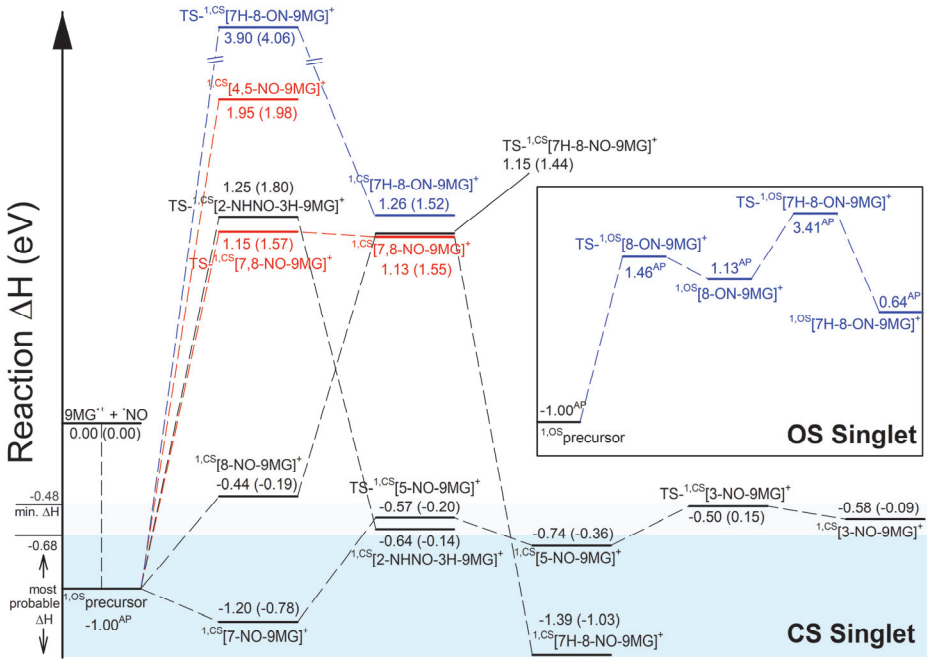


**Fig. 4.** Potential energy diagram for the reaction of $9MG^{\bullet+}$ + $^{\bullet}NO$ in the open- and closed-shell singlet states. Enthalpies (298 K) were calculated at CASPT2/ANO-L-VTZP//ωB97XD/6-31+G(d,p) and DLPNO-CCSD(T)/aug-cc-pVTZ //ωB97XD/6-31+G(d,p) (numbers in parentheses), except for open-shell singlet species which were calculated at AP-DFT (indicated with superscript AP). The shaded areas indicate the minimum and the most probable exothermicity range for experimentally measured product.

$^{1,CS}$[7-NO-9MG]$^+$ may continue conversion to $^{1,CS}$[5-NO-9MG]$^+$ and $^{1,CS}$[3-NO-9MG]$^+$ with barriers below the reactants. To determine relative contributions of different adduct structures, RRKM kinetics modeling was utilized. The time scale for interconversion between $^{1,CS}$[7-NO-9MG]$^+$ and $^{1,CS}$[5-NO-9MG]$^+$ is less than 0.1 ns at the $E_{CM}$ range of 0.05 – 0.2 eV, and that for interconversion between $^{1,CS}$[5-NO-9MG]$^+$ and $^{1,CS}$[3-NO-9MG]$^+$ is less than 1 ns at the same energy range. As a consequence, an equilibrium between $^{1,CS}$[3-NO-9MG]$^+$, $^{1,CS}$[5-NO-9MG]$^+$, and $^{1,CS}$[7-NO-9MG]$^+$ could be anticipated within the product ion time-of-flight. We could then use the ratio of DOS in these complexes to estimate their relative populations and determine which complexes are important. The DOS is energy-dependent. It turns out that, at $E_{CM} \leq 0.5$ eV, $^{1,CS}$[7-NO-9MG]$^+$ is predominant (> 99%); on the other hand, neither $^{1,CS}$[3-NO-9MG]$^+$ (0%) nor $^{1,CS}$[5-NO-9MG]$^+$ (< 0.1%) makes a meaningful contribution. Furthermore, the RRKM kinetics modeling predicted that $^{1,CS}$[7-NO-9MG]$^+$ has a lifetime of $10^2 – 10^3$ μs at $E_{CM}$ below 0.2 eV but decreased to less than μs at $E_{CM}$ above 0.5 eV. Therefore, while $^{1,CS}$[7-NO-9MG]$^+$ accounted

for the product ions at low energies; at high energies, it decomposed into starting reactants before reaching the mass spectrometer detector. Such kinetics rationalizes the quick decline of exothermic product ions with increasing kinetic energy in Figures 1–2.

Folkes and O′Neill[40] proposed the formation of $^{1,CS}$[2-NHNO-G] during the modification of DNA by •NO under ionizing radiation, which corresponds to $^{1,CS}$[2-NHNO-3H-9MG]$^+$ in the present reaction system. Despite this product being exothermic by 0.64 eV, it requires an activation barrier of 1.25 eV, making it less likely to occur in reality. Similarly, the product ion $^{1,CS}$[7H-8-NO-9MG]$^+$, although the most stable, requires a 1.15 eV activation energy above the reactants and is therefore insignificant.

Figure 4 also presents the two open-shell singlet products: $^{1,OS}$[8-ȮṄ-9MG]$^+$ and $^{1,OS}$[7H-8-ȮṄ-9MG]$^+$, neither of which is thermodynamically favorable. Note that none of the biradical cyclo-adducts were included in the figure for two reasons: biradical cyclo-adducts demand high energetics for formation, and in fact, all these structures converged to different (non-cyclic) structures in restricted closed-shell calculations — implying their inherent instability.[79]

**B. Origin of the minor, endothermic nitration product**

We now turn to the identification of the endothermic nitrosation product detected at $E_{CM}$ = 0.18 – 0.22 eV for dry 9MG•$^+$ + •NO (Figure 2a). It is evident in Figure 4 that the singlet product channels are either exothermic with no activation barrier above the reactants (such as $^{1,CS}$[3-NO-9MG]$^+$, $^{1,CS}$[5-NO-9MG]$^+$, $^{1,CS}$[7-NO-9MG]$^+$, and $^{1,CS}$[8-NO-9MG]$^+$) or have product endothermicity or activation barrier of at least 1.15 eV (such as the closed-shell $^{1,CS}$[2-NHNO-3H-9MG]$^+$, $^{1,CS}$[7H-8-NO-9MG]$^+$, $^{1,CS}$[7H-8-ON-9MG]$^+$, $^{1,CS}$[4,5-NO-9MG]$^+$ and $^{1,CS}$[7,8-NO-9MG]$^+$, and the open-shell $^{1,OS}$[8-ȮṄ-9MG]$^+$ and $^{1,OS}$[7H-8-ȮṄ-9MG]$^+$). Therefore, none of these would be relevant to a moderate endothermic reaction.

It follows that the detected endothermic product may only arise from a triplet state. Figure 5 outlines all triplet addition pathways initiated at $^3$precursor. All reactions present an activation barrier in the range of 0.73 – 3.38 eV, except for $^3$[8-NO-9MG]$^+$ which has a reaction enthalpy of 0.45 eV and an activation barrier of 0.62 eV. Therefore, $^3$[8-NO-9MG]$^+$ represents the most likely endothermic product structure in

the experiment. The fact that this channel was observed at the range of $E_{CM}$ (0.18 – 0.22 eV) below its calculated barrier was due to reactant internal energy and translational kinetic energy spread and Doppler broadening in ion-molecule collisions. The falloff of the $^3$[8-NO-9MG]$^+$ cross section at high energies is due to the combination of the decreasing complex intermediacy and the emerging of the spin-orbit charge transfer reaction.[27]

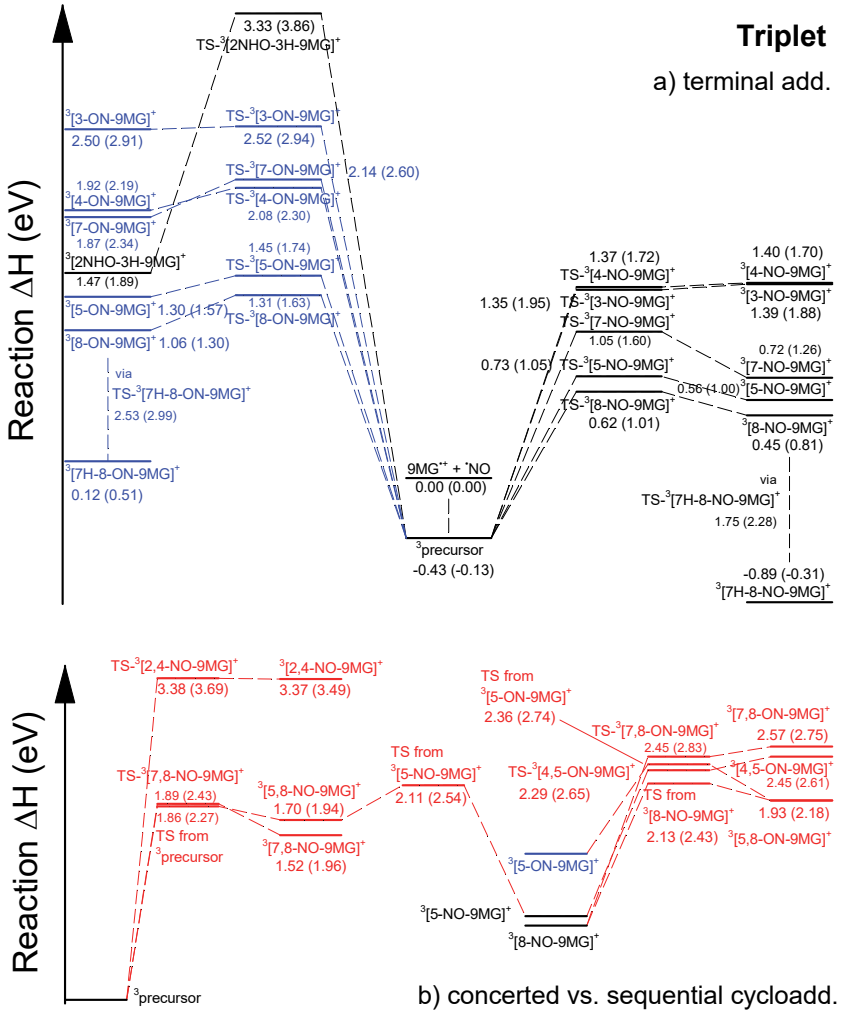


**Fig. 5.** Potential energetic diagram for the reaction of 9MG$^{\bullet+}$ + $^{\bullet}$NO in the triplet state. Enthalpies (298 K) were calculated at CASPT2/ANO-L-VTZP//ωB97XD/6-31+G(d,p) and DLPNO-CCSD(T)/aug-cc-pVTZ// ωB97XD/6-31+G(d,p) (numbers in parentheses).

## C. Low yield for radical-radical combination

The low nitrosation product yield for 9HG$^{\bullet+}$ and 9MG$^{\bullet+}$, even in the presence of hydration, warrants rationalization. The nitrosative reaction, or, in a general sense, combination of radicals, is spin

selective.[107] The pair of guanine radical cation and •NO can form one anti-symmetric, singlet spin eigenfunction $[\alpha(1)\beta(2) - \beta(1)\alpha(2)]/\sqrt{2}$, and three symmetric, triplet spin eigenfunctions $\alpha(1)\alpha(2)$, $\beta(1)\beta(2)$, and $[\alpha(1)\beta(2) + \beta(1)\alpha(2)]/\sqrt{2}$. Therefore, the partition between singlet and triplet is 0.25:0.75.

Nitration products may form from radical-radical combination to the lowest-energy triplet state. However, all triplet pathways are endothermic and face competition from CT as well as non-reactive collisions (i.e., escaping combination and decaying back to reactants), with these factors being cumulative. Of course, the triplet may interconvert to the singlet but must be driven by spin-orbit charge transfer-induced ISC;[27] consequently, the final state must correlate to CT products 9MG + $NO^+$. On the other hand, the charge in all nitrosation products remains predominantly localized at the 9MG moiety, thereby mitigating the driving force for the envisioned triplet-singlet transition (unless a spin flip is induced additionally by a heavy-atom substitute[108] and/or paramagnetic relaxation[109] ). That implies that, of all ion-molecule collisions, 75% which were born in the triplet could be largely discounted for nitrosation.

The combination of the radicals into a singlet state may occur without any activation barrier (Figure 4). It follows that a reaction yield of up to 25% could be expected at the lowest collision energy. This statement, however, was true only if all starting open-shell singlet ion-molecule encounters converged to closed-shell singlet and all singlet products were captured by the mass spectrometer. Unfortunately, the less-than-100% interconversion between open- and closed-shell singlets (due to reaction orientation dependence) as well as the fast decay of nascent, singlet nitrosation products have in turn invalidated this condition. The monohydration of reactant ions had helped a fraction of the product ions survive, but the effect was not substantial enough to reverse the prevailing trend toward decay.

**VI. Conclusions**

Following our previous study on the spin-orbit charge transfer of •NO with $9HG^{\bullet+}$ and $9MG^{\bullet+}$, we carried out a combined guided-ion beam mass spectrometry and electronic structure investigation of the

nitrosation reactions for these two reaction systems. $9HG^{\bullet+}$ and $9MG^{\bullet+}$ present similar reaction outcomes, and they are referred to collectively as $G^{\bullet+}$. Both open-shell singlet $^{1,OS}[G^{\bullet+}(\uparrow)\cdots(\downarrow)^{\bullet}NO]$ and triplet $^{3}[G^{\bullet+}(\uparrow)\cdots(\uparrow)^{\bullet}NO]$ formed reaction precursors in a ratio of 1:3. The $^{3}[G^{\bullet+}(\uparrow)\cdots(\uparrow)^{\bullet}NO]$ precursor is responsible for the formation of a minor amount of endothermic product ions $^{3}[8\text{-NO-G}]^{+}$ at relatively low collision energies and for the spin-orbit charge transfer at high energies. The $^{1,OS}[G^{\bullet+}(\uparrow)\cdots(\downarrow)^{\bullet}NO]$ precursor, on the other hand, leads to the ultimate formation of the major, exothermic product ions $^{1,CS}[7\text{-NO-G}]^{+}$ without any activation barriers above the reactants. Combined with our previous work, we have delineated the roles and evolution of the two charge states and three spin configurations and caught a glimpse of fertile radical-radical reaction dynamics. The findings have demonstrated synergistic oxidative nucleobase damage in the presence of ionization, one-electron oxidation, and nitrosation.

**Supplementary Material**

Cartesian coordinates, energetics, $\langle\widehat{S^2}\rangle$, and T1 diagnostic for all reaction structures.

**Acknowledgements**

This work was supported by the National Science Foundation (Grant No. CHE 2350109). JB acknowledges the CUNY Graduate Center Dissertation Fellowship and Doctoral Student Research Grant. TS acknowledges the Grant-in-Aid for Scientific Research (C) (No. 24K08357) from the Japan Society for the Promotion of Science.

**Data Availability**

The data that support the findings of this study are available within the article and its supplementary material.

**References**

[1] J. Zhou, O. Kostko, C. Nicolas, X. Tang, L. Belau, M. S. de Vries, and M. Ahmed,"Experimental observation of guanine tautomers with VUV photoionization," J. Phys. Chem. A **113**, 4829-4832 (2009).

[2] M. Schwell and M. Hochlaf,"Photoionization spectroscopy of nucleobases and analogues in the gas phase using synchrotron radiation as excitation light source," Top. Curr. Chem. **355**, 155-208 (2015).

[3] S. Steenken and S. V. Jovanovic,"How easily oxidizable is DNA? One-electron reduction potentials of adenosine and guanosine radicals in aqueous solution," J. Am. Chem. Soc. **119**, 617-618 (1997).

[4] C. J. Burrows and J. G. Muller,"Oxidative nucleobase modifications leading to strand scission," Chem. Rev. **98**, 1109-1151 (1998).

[5] L. P. Candeias and S. Steenken,"Ionization of purine nucleosides and nucleotides and their components by 193-nm laser photolysis in aqueous solution: Model studies for oxidative damage of DNA," J. Am. Chem. Soc. **114**, 699-704 (1992).

[6] D. N. Nikogosyan,"Two-quantum UV photochemistry of nucleic acids: Comparison with conventional low-

intensity UV photochemistry and radiation chemistry," Int. J. Radiat. Biol. **57**, 233-299 (1990).

[7] L. P. Candeias and S. Steenken,"Structure and acid-base properties of one-electron-oxidized deoxyguanosine, guanosine, and 1-methylguanosine," J. Am. Chem. Soc. **111**, 1094-1099 (1989).

[8] S. Steenken,"Purine bases, nucleosides, and nucleotides: Aqueous solution redox chemistry and transformation reactions of their radical cations and $e^-$ and OH adducts," Chem. Rev. **89**, 503-520 (1989).

[9] M. Kant, P. Jaruga, E. Coskun, S. Ward, A. D. Stark, T. Baumann, D. Becker, A. Adhikary, M. D. Sevilla, and M. Dizdaroglu,"Ne-22 ion-beam radiation damage to DNA: From initial free radical formation to resulting DNA-base damage," ACS Omega **6**, 16600-16611 (2021).

[10] I. Saito, T. Nakamura, and K. Nakatani,"Mapping of highest occupied molecular orbitals of duplex DNA by cobalt-mediated guanine oxidation," J. Am. Chem. Soc. **122**, 3001-3006 (2000).

[11] H. H. Thorp,"Cutting out the middleman: DNA biosensors based on electrochemical oxidation," Trends Biotechnol. **16**, 117-121 (1998).

[12] H. Kasai, Z. Yamaizumi, M. Berger, and J. Cadet,"Photosensitized formation of 7,8-dihydro-8-oxo-2'-deoxyguanosine (8-hydroxy-2'-deoxyguanosine) in DNA by riboflavin: A non singlet oxygen-mediated reaction," J. Am. Chem. Soc. **114**, 9692-9694 (1992).

[13] J. Cadet, T. Douki, and J.-L. Ravanat,"Oxidatively generated base damage to cellular DNA," Free Radic. Biol. Med. **49**, 9-21 (2010).

[14] J. Cadet and J. R. Wagner,"DNA base damage by reactive oxygen species, oxidizing agents, and UV radiation," Cold Spring Harbor Perspect. Biol. **5**, A012559 (2013).

[15] W. L. Neeley and J. M. Essigmann,"Mechanisms of formation, genotoxicity, and mutation of guanine oxidation products," Chem. Res. Toxicol. **19**, 491-505 (2006).

[16] A. M. Fleming and C. J. Burrows,"Formation and processing of DNA damage substrates for the hNEIL enzymes," Free Radic. Biol. Med. **107**, 35-52 (2017).

[17] D. Becker and M. D. Sevilla, in *Advances in radiation biology*, edited by J. T. Lett and W. K. Sinclair (Academic Press, Inc., San Diego, CA, 1993), pp. 121-180.

[18] M. D. Sevilla, D. Becker, A. Kumar, and A. Adhikary,"Gamma and ion-beam irradiation of DNA: Free radical mechanisms, electron effects, and radiation chemical track structure," Radiat. Phys. Chem. **128**, 60-74 (2016).

[19] D. T. Sawyer, *Oxygen chemistry* (Oxford University Press, New York, 1991),

[20] J. R. Lancaster,"Nitroxidative, nitrosative, and nitrative stress: Kinetic predictions of reactive nitrogen species chemistry under biological conditions," Chem. Res. Toxicol. **19**, 1160-1174 (2006).

[21] P. Kovacic and R. Somanathan,"Nitric oxide, peroxynitrite, peroxynitrous acid, nitroxyl, nitrogen dioxide, nitrous oxide: Biochemical mechanisms and bioaction," Curr. Bioact. Compd. **8**, 297-306 (2012).

[22] Y. Sun, M. Tsai, M. M. Moe, and J. Liu,"Dynamics and multiconfiguration potential energy surface for the singlet $O_2$ reactions with radical cations of guanine, 9-methylguanine, 2'-deoxyguanosine, and guanosine," J. Phys. Chem. A **125**, 1564-1576 (2021).

[23] M. M. Moe, M. Tsai, and J. Liu,"Singlet oxygen oxidation of the radical cations of 8-oxo-2'-deoxyguanosine and its 9-methyl analogue: Dynamics, potential energy surface, and products mediated by C5-$O_2$-addition," ChemPlusChem **86**, 1243-1254 (2021).

[24] J. Benny, T. Saito, M. M. Moe, and J. Liu,"Singlet $O_2$ reactions with radical cations of 8-bromoguanine and 8-bromoguanosine: Guided-ion beam mass spectrometric measurements and theoretical treatments," J. Phys. Chem. A **126**, 68-79 (2022).

[25] M. M. Moe, T. Saito, M. Tsai, and J. Liu,"Singlet $O_2$ oxidation of the radical cation versus the dehydrogenated neutral radical of 9-methylguanine in a Watson-Crick base pair. Consequences of structural context," J. Phys. Chem. B **126**, 5458-5472 (2022).

[26] M. M. Moe, M. Tsai, and J. Liu,"Effects of intra-base pair proton transfer on dissociation and singlet oxygenation of 9-methyl-8-oxoguanine-1-methyl-cytosine base-pair radical cation," ChemPhysChem **24**, e202300511 (2023).

[27] J. Benny and J. Liu,"Spin-orbit charge transfer from guanine and 9-methylguanine radical cations to nitric oxide radicals and the induced triplet-to-singlet intersystem crossing," J. Chem. Phys. **159**, 085102 (2023).

[28] P. Howard-Flanders,"Effect of nitric oxide on the radiosensitivity of bacteria," Nature **180**, 1191-1192 (1957).

[29] L. H. Gray, F. O. Green, and C. A. Hawes,"The effect of nitric oxide on the radiosensitivity of tumor cells," Nature **182**, 952-953 (1958).

[30] D. L. Dewey,"Effect of oxygen and nitric oxide on the radiosensitivity of human cells in tissue culture," Nature **186**, 780-782 (1960).

[31] J. B. Mitchell, D. A. Wink, W. DeGraff, J. Gamson, L. K. Keefer, and M. C. Krishna,"Hypoxic mammalian cell radiosensitization by nitric oxide," Cancer Res. **53**, 5845-5848 (1993).

[32] R. J. Griffin, C. M. Makepeace, W. J. Hur, and C. W. Song,"Radiosensitization of hypoxic tumor cells in vitro by nitric oxide," Int. J. Radiat. Oncol. Biol. Phys. **36**, 377-383 (1996).

[33] B. F. Jordan, P. Sonveaux, O. Feron, V. Grégoire, N. Beghein, C. Dessy, and B. Gallez,"Nitric oxide as a radiosensitizer: Evidence for an intrinsic role in addition to its effect on oxygen delivery and consumption," Int. J. Cancer **109**, 768-773 (2004).

[34] P. Wardman, K. Rothkamm, L. K. Folkes, M. Woodcock, and P. J. Johnston,"Radiosensitization by nitric oxide at low radiation doses," Radiat. Res. **167**, 475-484 (2007).

[35] G. D. Stewart, J. Nanda, E. Katz, K. J. Bowman, J. G. Christie, D. J. G. Brown, D. B. McLaren, A. C. P. Riddick, J. A. Ross, G. D. D. Jones, and F. K. Habib,"DNA strand breaks and hypoxia response inhibition mediate the radiosensitisation effect of nitric oxide donors on prostate cancer under varying oxygen conditions," Biochem. Pharmacol. **81**, 203-210 (2011).

[36] S. Ning, M. Bednarski, B. Oronsky, J. Scicinski, G. Saul, and S. J. Knox,"Dinitroazetidines are a novel class of anticancer agents and hypoxia-activated radiation sensitizers developed from highly energetic materials," Cancer Res. **72**, 2600-2608 (2012).

[37] L. K. Folkes and P. O'Neill,"DNA damage induced by nitric oxide during ionizing radiation is enhanced at replication," Nitric Oxide **34**, 47-55 (2013).

[38] J. Tu, K. Tu, H. Xu, L. Wang, X. Yuan, X. Qin, L. Kong, Q. Chu, and Z. Zhang,"Improving tumor hypoxia and radiotherapy resistance via in situ nitric oxide release strategy," Eur. J. Pharm. Biopharm. **150**, 96-107 (2020).

[39] L. K. Keefer and D. A. Wink, in *Biological reactive intermediates v: Basic mechanistic research in toxicology and human risk assessment*, edited by R. Snyder *et al.* (Springer US, Boston, MA, 1996), pp. 177-185.

[40] L. K. Folkes and P. O'Neill,"Modification of DNA damage mechanisms by nitric oxide during ionizing radiation," Free Radic. Biol. Med. **58**, 14-25 (2013).

[41] W. Klopper, J. Noga, H. Koch, and T. Helgaker,"Multiple basis sets in calculations of triples corrections in coupled-cluster theory," Theo. Chem. Acc. **97**, 164-176 (1997).

[42] M. Pitoňák, F. Holka, P. Neogrády, and M. Urban,"Optimized virtual orbitals for correlated calculations: Towards large scale CCSD(T) calculations of molecular dipole moments and polarizabilities," J. Mol. Struc. Theochem **768**, 79-89 (2006).

[43] J. Řezáč and P. Hobza,"Describing noncovalent interactions beyond the common approximations: How accurate is the "gold standard," CCSD(T) at the complete basis set limit?," J. Chem. Theo. Comput. **9**, 2151-2155 (2013).

[44] J. Olsen, B. O. Roos, P. Jøgensen, and H. J. A. Jensen,"Determinant based configuration interaction algorithms for complete and restricted configuration interaction spaces," J. Chem. Phys. **89**, 2185-2192 (1988).

[45] B. O. Roos, P. R. Taylor, and E. M. Siegbahn,"A complete active space scf method (CASSCF) using a density matrix formulated super-CI approach," Chem. Phys. **48**, 157-173 (1980).

[46] J. J. W. McDouall, K. Peasley, and M. A. Robb,"A simple MC SCF perturbation theory: Orthogonal valence bond Møller-Plesset 2 (OVB MP2)," Chem. Phys. Lett. **148**, 183-189 (1988).

[47] K. Andersson, P. A. Malmqvist, B. O. Roos, A. J. Sadlej, and K. Wolinski,"Second-order perturbation theory with a CASSCF reference function," J. Phys. Chem. **94**, 5483-5488 (1990).

[48] K. Andersson, P. A. Malmqvist, and B. O. Roos,"Second-order perturbation theory with a complete active space self-consistent field reference function," J. Chem. Phys. **96**, 1218-1226 (1992).

[49] M. Abe, G. Gopakmar, T. Nakajima, and K. Hirao, in *Radiation induced molecular phenomena in nucleic acids*, edited by K. Shukla, M. K., and J. Leszczynski (Springer, Netherlands, 2008), pp. 157-177.

[50] Y. Fang and J. Liu,"Reaction of protonated tyrosine with electronically excited singlet molecular oxygen ($a^1\Delta_g$): An experimental and trajectory study," J. Phys. Chem. A **113**, 11250-11261 (2009).

[51] I. K. Chu, C. F. Rodriquez, T.-C. Lau, A. C. Hopkinson, and K. W. M. Siu,"Molecular radical cations of oligopeptides," J. Phys. Chem. B **104**, 3393-3397 (2000).

[52] L. Feketeová, E. Yuriev, J. D. Orbell, G. N. Khairallah, and R. A. J. O'Hair,"Gas-phase formation and reactions of radical cations of guanosine, deoxyguanosine and their homodimers and heterodimers," Int. J. Mass Spectrom. **304**,

74-82 (2011).

[53] P. Cheng and D. K. Bohme,"Gas-phase formation of radical cations of monomers and dimers of guanosine by collision-induced dissociation of Cu(II)-guanosine complexes," J. Phys. Chem. B **111**, 11075-11082 (2007).

[54] L. Feketeová, B. Chan, G. N. Khairallah, V. Steinmetz, P. Maitre, L. Radom, and R. A. J. O'Hair,"Watson–Crick base pair radical cation as a model for oxidative damage in DNA," J. Phys. Chem. Lett. **8**, 3159-3165 (2017).

[55] A. Dang, Y. Liu, and F. Tureček,"UV-Vis action spectroscopy of guanine, 9-methylguanine, and guanosine cation radicals in the gas phase," J. Phys. Chem. A **123**, 3272-3284 (2019).

[56] A. N. Krutchinsky, I. V. Chernushevich, V. L. Spicer, W. Ens, and K. G. Standing,"Collisional damping interface for an electrospray ionization time-of-flight mass spectrometer," J. Am. Soc. Mass Spectrom. **9**, 569-579 (1998).

[57] D. J. Douglas and J. B. French,"Collisional focusing effects in radio frequency quadrupoles," J. Am. Mass Spectrom. **3**, 398-408 (1992).

[58] K. M. Ervin and P. B. Armentrout,"Translational energy dependence of $Ar^+ + XY \rightarrow ArX^+ + Y$ ($XY = H_2, D_2, HD$) from thermal to 30 eV c.m.," J. Chem. Phys. **83**, 166-189 (1985).

[59] P. B. Armentrout,"Kinetic energy dependence of ion-molecule reactions: Guided ion beams and threshold measurement," Int. J. Mass Spectrom. **200**, 219-241 (2000).

[60] P. B. Armentrout,"Fundamental of ion-molecule chemistry," J. Anal. At. Spectrom. **19**, 571-580 (2004).

[61] A. Kumar and M. D. Sevilla,"Proton transfer induced somo-to-homo level switching in one-electron oxidized A-T and G-C base pairs: A density functional theory study," J. Phys. Chem. B **118**, 5453-5458 (2014).

[62] M. C. Aragoni, C. Caltagirone, V. Lippolis, E. Podda, A. M. Z. Slawin, J. D. Woollins, A. Pintus, and M. Arca,"Diradical character of neutral heteroleptic bis(1,2-dithiolene) metal complexes: Case study of [Pd($Me_2$timdt)(mnt)] ($Me_2$timdt = 1,3-dimethyl-2,4,5-trithioxoimidazolidine; $mnt^{2-}$ = 1,2-dicyano-1,2-ethylenedithiolate)," Inorg. Chem. **59**, 17385-17401 (2020).

[63] M. J. Frisch, G. W. Trucks, H. B. Schlegel, G. E. Scuseria, M. A. Robb, J. R. Cheeseman, G. Scalmani, V. Barone, G. A. Petersson, H. Nakatsuji, X. Li, M. Caricato, A. V. Marenich, J. Bloino, B. G. Janesko, R. Gomperts, B. Mennucci, H. P. Hratchian, J. V. Ortiz, A. F. Izmaylov, J. L. Sonnenberg, D. Williams-Young, F. Ding, F. Lipparini, F. Egidi, J. Goings, B. Peng, A. Petrone, T. Henderson, D. Ranasinghe, V. G. Zakrzewski, J. Gao, N. Rega, G. Zheng, W. Liang, M. Hada, M. Ehara, K. Toyota, R. Fukuda, J. Hasegawa, M. Ishida, T. Nakajima, Y. Honda, O. Kitao, H. Nakai, T. Vreven, K. Throssell, J. A. Montgomery Jr., J. E. Peralta, F. Ogliaro, M. J. Bearpark, J. J. Heyd, E. N. Brothers, K. N. Kudin, V. N. Staroverov, T. A. Keith, R. Kobayashi, J. Normand, K. Raghavachari, A. P. Rendell, J. C. Burant, S. S. Iyengar, J. Tomasi, M. Cossi, J. M. Millam, M. Klene, C. Adamo, R. Cammi, J. W. Ochterski, R. L. Martin, K. Morokuma, O. Farkas, J. B. Foresman, and D. J. Fox, Gaussian 16 Gaussian, Inc., 2016.

[64] I. M. Alecu, J. Zheng, Y. Zhao, and D. G. Truhlar,"Computational thermochemistry: Scale factor databases and scale factors for vibrational frequencies obtained from electronic model chemistries," J. Chem. Theory Comput. **6**, 2872-2887 (2010).

[65] E. D. Glendening, J. K. Badenhoop, A. E. Reed, J. E. Carpenter, J. A. Bohmann, C. M. Morales, C. R. Landis, and F. Weinhold, NBO 6.0, Theoretical Chemistry Institute, University of Wiscosin, 2013.

[66] P. G. Szalay, J. Vazquez, C. Simmons, and J. F. Stanton,"Triplet instability in doublet systems," J. Chem. Phys. **121**, 7624-7631 (2004).

[67] M.-P. Kitsaras and S. Stopkowicz,"Spin contamination in MP2 and CC2, a surprising issue," J. Chem. Phys. **154**, 131101 (2021).

[68] G. K. Jarvis, M. Evans, C. Y. Ng, and K. Mitsuke,"Rotational-resolved pulsed field ionization photoelectron study of $NO^+(X\,^1\Sigma^+, v^+=0–32)$ in the energy range of 9.24–16.80 eV," J. Chem. Phys. **111**, 3058-3069 (1999).

[69] T. J. Lee and P. R. Taylor,"A diagnostic for determining the quality of single-reference electron correlation methods," Int. J. Quantum Chem., Quantum Chem. Symp. **36**, 199-207 (1989).

[70] D. Jayatilaka and T. J. Lee,"Open-shell, coupled-cluster theory," J. Chem. Phys. **98**, 9734-9747 (1993).

[71] C. Riplinger, B. Sandhoefer, A. Hansen, and F. Neese,"Natural triple excitations in local coupled cluster calculations with pair natural orbitals," J. Chem. Phys. **139**, (2013).

[72] Y. Guo, C. Riplinger, U. Becker, D. G. Liakos, Y. Minenkov, L. Cavallo, and F. Neese,"Communication: An improved linear scaling perturbative triples correction for the domain based local pair-natural orbital based singles and doubles coupled cluster method [DLPNO-CCSD(T)]," J. Chem. Phys. **148**, (2018).

[73] S. Mallick, B. Roy, and P. Kumar,"A comparison of DLPNO-CCSD(T) and CCSD(T) method for the determination of the energetics of hydrogen atom transfer reactions," Comput. Theor. Chem. **1187**, 112934 (2020).

[74] D. G. Liakos, M. Sparta, M. K. Kesharwani, J. M. L. Martin, and F. Neese,"Exploring the accuracy limits of local pair natural orbital coupled-cluster theory," J. Chem. Theory Comput. **11**, 1525-1539 (2015).

[75] E. Paulechka and A. Kazakov,"Efficient DLPNO–CCSD(T)-based estimation of formation enthalpies for C-, H-, O-, and N-containing closed-shell compounds validated against critically evaluated experimental data," J. Phys. Chem. A **121**, 4379-4387 (2017).

[76] D. G. Liakos, Y. Guo, and F. Neese,"Comprehensive benchmark results for the domain based local pair natural orbital coupled cluster method (DLPNO-CCSD(T)) for closed- and open-shell systems," J. Phys. Chem. A **124**, 90-100 (2020).

[77] F. Neese,"The ORCA program system," Wiley Interdiscip. Rev.: Comput. Mol. Sci. **2**, 73-78 (2012).

[78] F. Neese,"Software update: The ORCA program system, version 4.0," WIREs Comput. Mol. Sci. **8**, e1327 (2018).

[79] P. D. Miller, D. A. Shultz, J. Mengell, M. L. Kirk, and L. Wojtas,"Variation from closed-shell to open shell electronic structures in oligothiophene bis(dioxolene) complexes," Chem. Sci. **14**, 12264-12276 (2023).

[80] K. Yamaguchi, F. Jensen, A. Dorigo, and K. N. Houk,"A spin-correction procedure for unrestricted Hartree-Fock and Møller-plesset wave functions for singlet diradicals and polyradicals," Chem. Phys. Lett. **149**, 537-542 (1988).

[81] T. Saito, S. Nishihara, Y. Kataoka, Y. Nakanishi, T. Matsui, Y. Kitagawa, T. Kawakami, M. Okumura, and K. Yamaguchi,"Transition state optimization based on approximate spin-projection (AP) method," Chem. Phys. Lett. **483**, 168-171 (2009).

[82] T. Saito, S. Nishihara, Y. Kataoka, Y. Nakanishi, Y. Kitagawa, T. Kawakami, S. Yamanaka, M. Okumura, and K. Yamaguchi,"Reinvestigation of the reaction of ethylene and singlet oxygen by the approximate spin projection method. Comparison with multireference coupled-cluster calculations," J. Phys. Chem. A **114**, 7967-7974 (2010).

[83] B. O. Roos, R. Lindh, P.-Å. Malmqvist, V. Veryazov, and P.-O. Widmark,"Main group atoms and dimers studied with a new relativistic ANO basis set," J. Phys. Chem. A **108**, 2851-2858 (2004).

[84] B. O. Roos, R. Lindh, P.-Å. Malmqvist, V. Veryazov, and P.-O. Widmark,"New relativistic ANO basis sets for transition metal atoms," J. Phys. Chem. A **109**, 6575-6579 (2005).

[85] B. O. Roos and K. Andersson,"Multiconfigurational perturbation theory with level shift — the $Cr_2$ potential revisited," Chem. Phys. Lett. **245**, 215-223 (1995).

[86] N. Forsberg and P.-Å. Malmqvist,"Multiconfiguration perturbation theory with imaginary level shift," Chem. Phys. Lett. **274**, 196-204 (1997).

[87] D. Roca-Sanjuán, M. Rubio, M. Merchán, and L. Serrano-Andrés,"Ab initio determination of the ionization potentials of DNA and RNA nucleobases," J. Chem. Phys. **125**, 084302 (2006).

[88] G. Ghigo, B. O. Roos, and P.-Å. Malmqvist,"A modified definition of the zeroth-order hamiltonian in multiconfigurational perturbation theory (CASPT2)," Chem. Phys. Lett. **396**, 142-149 (2004).

[89] P.-O. Widmark, P.-Å. Malmqvist, and B. O. Roos,"Density matrix averaged atomic natural orbital (ANO) basis sets for correlated molecular wave functions," Theor. Chim. Acta **77**, 291-306 (1990).

[90] P.-O. Widmark, J. P. Zobel, V. P. Vysotskiy, T. Tsuchiya, and V. Veryazov,"New compact density matrix averaged ANO basis sets for relativistic calculations," J. Chem. Phys. **149**, (2018).

[91] B. P. Pritchard, D. Altarawy, B. Didier, T. D. Gibson, and T. L. Windus,"New basis set exchange: An open, up-to-date resource for the molecular sciences community," J. Chem. Inf. Model. **59**, 4814-4820 (2019).

[92] I. Fdez. Galván, M. Vacher, A. Alavi, C. Angeli, F. Aquilante, J. Autschbach, J. J. Bao, S. I. Bokarev, N. A. Bogdanov, R. K. Carlson, L. F. Chibotaru, J. Creutzberg, N. Dattani, M. G. Delcey, S. S. Dong, A. Dreuw, L. Freitag, L. M. Frutos, L. Gagliardi, F. Gendron, A. Giussani, L. González, G. Grell, M. Guo, C. E. Hoyer, M. Johansson, S. Keller, S. Knecht, G. Kovačević, E. Källman, G. Li Manni, M. Lundberg, Y. Ma, S. Mai, J. P. Malhado, P. Å. Malmqvist, P. Marquetand, S. A. Mewes, J. Norell, M. Olivucci, M. Oppel, Q. M. Phung, K. Pierloot, F. Plasser, M. Reiher, A. M. Sand, I. Schapiro, P. Sharma, C. J. Stein, L. K. Sørensen, D. G. Truhlar, M. Ugandi, L. Ungur, A. Valentini, S. Vancoillie, V. Veryazov, O. Weser, T. A. Wesołowski, P.-O. Widmark, S. Wouters, A. Zech, J. P. Zobel, and R. Lindh,"Openmolcas: From source code to insight," J. Chem. Theory Comput. **15**, 5925-5964 (2019).

[93] G. Li Manni, I. Fdez. Galván, A. Alavi, F. Aleotti, F. Aquilante, J. Autschbach, D. Avagliano, A. Baiardi, J. J. Bao, S. Battaglia, L. Birnoschi, A. Blanco-González, S. I. Bokarev, R. Broer, R. Cacciari, P. B. Calio, R. K. Carlson, R. Carvalho Couto, L. Cerdán, L. F. Chibotaru, N. F. Chilton, J. R. Church, I. Conti, S. Coriani, J. Cuéllar-Zuquin, R. E. Daoud, N. Dattani, P. Decleva, C. de Graaf, M. G. Delcey, L. De Vico, W. Dobrautz, S. S. Dong, R. Feng, N. Ferré, M. Filatov, L. Gagliardi, M. Garavelli, L. González, Y. Guan, M. Guo, M. R. Hennefarth, M. R. Hermes, C. E.

Hoyer, M. Huix-Rotllant, V. K. Jaiswal, A. Kaiser, D. S. Kaliakin, M. Khamesian, D. S. King, V. Kochetov, M. Krośnicki, A. A. Kumaar, E. D. Larsson, S. Lehtola, M.-B. Lepetit, H. Lischka, P. López Ríos, M. Lundberg, D. Ma, S. Mai, P. Marquetand, I. C. D. Merritt, F. Montorsi, M. Mörchen, A. Nenov, V. H. A. Nguyen, Y. Nishimoto, M. S. Oakley, M. Olivucci, M. Oppel, D. Padula, R. Pandharkar, Q. M. Phung, F. Plasser, G. Raggi, E. Rebolini, M. Reiher, I. Rivalta, D. Roca-Sanjuán, T. Romig, A. A. Safari, A. Sánchez-Mansilla, A. M. Sand, I. Schapiro, T. R. Scott, J. Segarra-Martí, F. Segatta, D.-C. Sergentu, P. Sharma, R. Shepard, Y. Shu, J. K. Staab, T. P. Straatsma, L. K. Sørensen, B. N. C. Tenorio, D. G. Truhlar, L. Ungur, M. Vacher, V. Veryazov, T. A. Voß, O. Weser, D. Wu, X. Yang, D. Yarkony, C. Zhou, J. P. Zobel and R. Lindh,"The Openmolcas web: A community-driven approach to advancing computational chemistry," J. Chem. Theory Comput. **19**, 6933-6991 (2023).

**94** R. A. Marcus,"Unimolecular dissociations and free radical recombination reactions," J. Chem. Phys. **20**, 359-364 (1952).

**95** T. Beyer and D. F. Swinehart,"Algorithm 448: Number of multiply-restricted partitions," Commun. ACM **16**, 379 (1973).

**96** L. Zhu and W. L. Hase, A general RRKM program (QCPE 644), quantum chemistry program exchange, Chemistry Department, University of Indiana, 1993.

**97** M. T. Rodgers, K. M. Ervin, and P. B. Armentrout,"Statistical modeling of collision-induced dissociation thresholds," J. Chem. Phys. **106**, 4499-4508 (1997).

**98** Y. Sun, W. Zhou, M. M. Moe, and J. Liu,"Reactions of water with radical cations of guanine, 9-methylguanine, 2'-deoxyguanosine and guanosine: Keto-enol isomerization, C8-hydroxylation, and effects of N9-substitution," Phys. Chem. Chem. Phys. **20**, 27510-27522 (2018).

**99** F. Rogalewicz, G. Louazel, Y. Hoppilliard, and G. Ohanessian,"Structures and fragmentations of electrosprayed Zn(II) complexes of carboxylic acids in the gas phase: Isomerisation versus desolvation during the last desolvation step," Int. J. Mass Spectrom. **228**, 779-795 (2003).

**100** Y. Sun, M. M. Moe, and J. Liu,"Mass spectrometry and computational study of collision-induced dissociation of 9-methylguanine-1-methylcytosine base-pair radical cation: Intra-base-pair proton transfer and hydrogen transfer, non-statistical dissociation, and reaction with a water ligand," Phys. Chem. Chem. Phys. **22**, 14875-14888 (2020).

**101** M. M. Moe, J. Benny, and J. Liu,"Collision-induced dissociation of homodimeric and heterodimeric radical cations of 9-methylguanine and 9-methyl-8-oxoguanine: Correlation between intra-base pair proton transfer originating from the N1–H at a Watson–Crick edge and non-statistical dissociation," Phys. Chem. Chem. Phys. **24**, 9263-9276 (2022).

**102** J. Troe," Statistical adiabatic channel model of ion-neutral dipole capture rate constants," Chem. Phys. Lett. **122**, 425-430 (1985).

**103** C. Larriba and C. J. Hogan, Jr.,"Free molecular collision cross section calculation methods for nanoparticles and complex ions with energy accommodation," J. Comput. Phys. **251**, 344-363 (2013).

**104** C. Larriba-Andaluz and C. J. Hogan, Jr.,"Collision cross section calculations for polyatomic ions considering rotating diatomic/linear gas molecules," J. Chem. Phys. **141**, 194107 (2014).

**105** W. Lu and J. Liu,"Capturing transient endoperoxide in the singlet oxygen oxidation of guanine," Chem. Eur. J. **22**, 3127-3138 (2016).

**106** W. Zhou and J. Liu,"Reaction mechanism and dynamics for C8-hydroxylation of 9-methylguanine radical cation by water molecules," Phys. Chem. Chem. Phys. **23**, 24464-24477 (2021).

**107** K. L. Ivanov, A. Wagenpfahl, C. Deibel, and J. Matysik,"Spin-chemistry concepts for spintronics scientists," Beilstein J. Nanotechnol. **8**, 1427-1445 (2017).

**108** D. S. McClure,"Triplet-Singlet transitions in organic molecules. Lifetime measurements of the triplet state," J. Chem. Phys. **17**, 905-913 (2004).

**109** K. Lüders and K. M. Salikhov,"Theoretical treatment of the recombination probability of radical pairs with consideration of singlet-triplet transitions induced by paramagnetic relaxation," Chem. Phys. **117**, 113-131 (1987).